J Biol Inorg Chem (2008) 13:1197–1204
DOI 10.1007/s00775-008-0403-6

ORIGINAL PAPER

Computational study of the binding of Cu^{II} to Alzheimer's amyloid-β peptide: Do Aβ42 and Aβ40 bind copper in identical fashion?

Yogita Mantri · Marco Fioroni · Mu-Hyun Baik

Received: 29 April 2008 / Accepted: 25 June 2008 / Published online: 8 July 2008
© SBIC 2008

Abstract One of the many hypotheses on the pathogenesis of Alzheimer's disease is that the amyloid-β peptide (Aβ) binds Cu^{II} and can catalytically generate H_2O_2, leading to oxidative damage in brain tissues. For a molecular level understanding of such catalysis it is critical to know the structure of the Aβ–Cu^{II} complex precisely. Unfortunately, no high-resolution structure is available to date and there is considerable debate over the copper coordination environment with no clear consensus on which residues are directly bound to Cu^{II}. Considering all plausible isomers of the copper-bound Aβ42 and Aβ40 using a combination of density functional theory and classical molecular dynamics methods, we report an atomic resolution structure for each possible complex. We evaluated the relative energies of these isomeric structures and surprisingly found that Aβ42 and Aβ40 display very different binding modes, suggesting that shorter peptides that are truncated at the C-terminus may not be realistic models for understanding the chemistry of the most neurotoxic peptide, Aβ42.

Keywords Copper–Aβ42 binding · Alzheimer's disease · Combined quantum mechanical (density functional theory)–classical molecular dynamics simulations · Copper–peptide binding energies

Electronic supplementary material The online version of this article (doi:10.1007/s00775-008-0403-6) contains supplementary material, which is available to authorized users.

Y. Mantri · M. Fioroni · M.-H. Baik (✉)
Department of Chemistry and School of Informatics,
Indiana University,
Bloomington,
IN 47405, USA
e-mail: mbaik@indiana.edu

Abbreviations

Aβ	Amyloid-β peptide
AD	Alzheimer's disease
DFT	Density functional theory
EPR	Electron paramagnetic resonance
MD	Molecular dynamics
MM	Molecular mechanics
QM	Quantum mechanical

Introduction

Alzheimer's disease (AD) is associated with insoluble, fibrillous plaques in brain tissues [1–3] consisting of amyloid-β peptides (Aβ). High concentrations of Cu^{II} and Zn^{II} have been found in the vicinity of the plaques isolated from postmortem brain tissue [4–6]. In addition, the tissues often display evidence of widespread oxidative damage such as lipid and protein peroxidation. Thus, among the many proposals for the pathogenesis of AD is the hypothesis that Aβ binds metal ions, in particular the redox-active Cu^{II} ion, and that the copper–Aβ complex in the fibrils catalytically activates dioxygen to generate hydrogen peroxide in the presence of reducing agents, which ultimately causes oxidative damage [7, 8]. Aβs are metabolites of a common protein, the amyloid precursor protein, the physiological function of which is currently not agreed upon. Whereas the structure of the amyloid precursor protein has been determined [9, 10], the exact structure of Aβ in neuritic plaques is not known. The most neurotoxic Aβ is 42 residues long, with only the first 16 amino acids being involved in copper binding [11]. Electronic paramagnetic resonance (EPR) spectroscopic studies suggest, not surprisingly, that the Cu^{II} center is four-coordinate with three nitrogen atoms and one

oxygen atom directly bound (3N1O) [12, 13]. The nitrogen ligands are thought to be histidine residues 6, 13, and 14 [13, 14], but the fourth, oxygen-donor ligand has proven difficult to identify.

Although many AD-related theoretical studies have been reported [15–29], the lack of precise structural data concerning the copper coordination makes atomistic inquiries related to the reactivity of the copper–Aβ complex difficult. Moreover, to our knowledge, there have been no atomistic theoretical studies on the copper–Aβ complex in the fibril environment, which is presumably responsible for concentrating copper and generating significantly larger amounts of hydrogen peroxide than copper–Aβ in solution. Using mutagenesis studies and EPR spectroscopy, Karr et al. [11] proposed that the first three amino acids are required for copper coordination as in the native peptide, with Asp1 suggested to play a major role. On the other hand, Tyr10 has been proposed to be the fourth ligand to copper on the basis of Raman spectroscopy [30], and a mechanism for the generation of hydrogen peroxide mediated by the copper–Aβ complex has been put forth using that model [8]. Tyr10 has also been shown to form dityrosine cross-links between two monomers after being oxidized, thus accelerating the formation of oligomers in these peptides [31]. High-resolution computer models can potentially make helpful contributions to this ongoing discussion by providing plausible structures and energetic comparisons of putative copper–Aβ complexes. Moreover, several studies have used shorter C-terminally truncated versions of full-length Aβ42, such as Aβ40, Aβ28, and Aβ16, on the basis of similarity in the EPR spectra of their copper-bound forms [11, 13, 32]. On the other hand, the aggregation behavior of these peptides is known to be different. In particular, studies comparing Aβ42 and Aβ40 suggest that truncating two amino acids results in dramatically different aggregation properties [24, 33, 34]. Thus, one goal of this work was to determine if there are differences in the copper binding modes of Aβ42 and Aβ40, either supporting or refuting the assumption that the shorter peptides can accurately capture the chemistry of Aβ42.

Constructing a realistic computer model of the copper–Aβ complex is challenging. High-level quantum mechanical (QM) methods are required for describing the coordination of copper, but the size of the system makes full QM treatment impractical. On the other hand, the flexibility of Aβ demands molecular dynamics (MD) methods to access realistic average structures at room temperature. Force fields for MD simulations based on classical molecular mechanics (MM) are not routinely available for copper complexes, however. To overcome these challenges, we used a hierarchical approach wherein small-model density functional theory (DFT) calculations were utilized to obtain the geometry and energetics for copper–ligand coordination, and these results were also used to build force fields for classical MD simulations of the full copper-bound peptide (Fig. 1a). The sequence of the first 16 amino acids (DAEFRHDSGYEVHHQK), which houses the native copper binding domain, allows for seven possible oxygen-donor ligands: Asp1, Asp7, Glu3, Glu11, Ser8, Tyr10, and Gln15. We systematically probed for each of these possibilities and compared them by combining energy components from both small-model QM and classical full-model MD simulations. Given the challenges and difficulties discussed above, it is imperative that we do not overinterpret our results. While precautions have been taken to make our computer models as consistent and robust as possible, the lack of experimental benchmark data and the intrinsic uncertainties of the underlying modeling techniques demand that we examine our numerical results with care and attempt to extract chemically reasonable and intuitively plausible trends and concepts rather than rely on predictions of absolute numeric value, such as thermodynamic properties. The ultimate target is to generate a structural model that is required for exploring the reactivity of the copper–Aβ complex in a systematic fashion using quantum chemical methods. The current structural and energetic analysis for binding Cu^{II} to Aβ42 and Aβ40 suggests that the two peptides prefer very different copper binding modes.

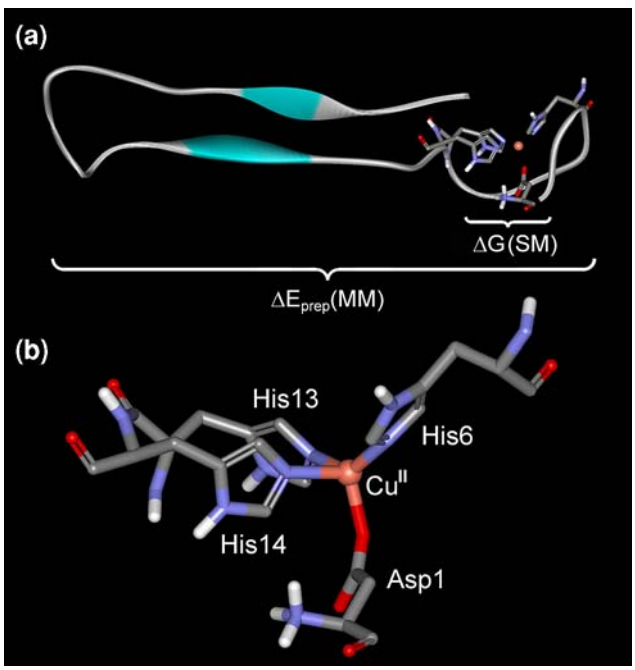

Fig. 1 Hierarchical approach used in modeling Cu–Aβ42 and Cu–Aβ40 complexes. *SM* small model, *MM* molecular mechanics

Methods

Small-model QM calculations

DFT has emerged as the QM method of choice for realistic simulations of systems as large as 150 atoms using a relatively high level of theory. Even so, this limit is still much smaller than the total size of the copper–Aβ complex. Therefore, smaller models were constructed using only the immediate coordination environment of copper for the high-level calculations. A representative of the small minimalist model is shown in Fig. 2. Only the copper atom and the amino acid side chains directly bound to copper were included in these calculations. To reduce the computational cost, amino acids were terminated at the Cα position, with the amine and carboxyl groups replaced by protons.

All calculations were carried out using DFT [35] as implemented in the Jaguar 5.5 suite [36] of quantum chemistry programs. Geometries were optimized by using the B3LYP [37–39] functional with the 6-31G** basis set. Copper was represented by the Los Alamos LACVP basis [40]. The energies were reevaluated by additional single-point calculations at each optimized geometry using Dunning's correlation-consistent triple-ζ basis set [41] cc-pVTZ(-f) with the standard double set of polarization functions. In these single-point calculations, copper was described by a modified version of LACVP, designated as LACV3P, where the exponents were decontracted to match the effective core potential with the triple-ζ quality basis. Vibrational frequency calculation results based on analytical second derivatives at the B3LYP/6-31G**/LACVP level of theory were used to confirm proper convergence to local minima and to derive the zero-point-energy and vibrational-entropy corrections at room temperature using unscaled frequencies. Because our small models consisted of four ligands and copper forming a single complex, the entropic penalty is expected to be very high. In reality, however, the four amino acids are linked in the peptide chain, thus decreasing the entropic penalty substantially. We, therefore, made the approximation that the translational and rotational components of entropy would be very similar in the free and copper-bound peptides, and included only the vibrational entropies for the ligands. On the other hand, the vibrational entropy of the copper-bound peptide is expected to increase owing to the greater vibrational degree of freedom afforded by the weakened Cα-backbone bonds of the copper ligands. Quantifying these properties is challenging, but since we are mainly interested in differential energies, we can reasonably assume some systematic error cancelation and ignore these effects in all peptides to a first-order approximation. Since the Cu^{II} ion is considered free before binding, we computed its entropy using the Sackur–Tetrode equation for the unbound state.

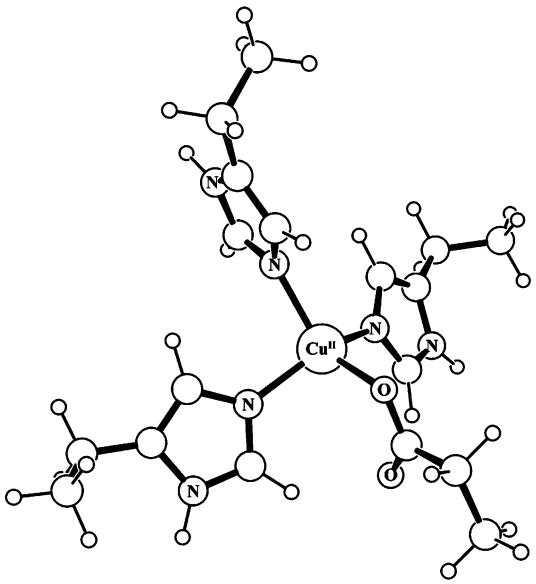

Fig. 2 Sample small model used for quantum mechanical simulations

Solvation energies were evaluated by a self-consistent reaction field approach with a solvent-excluding surface cavity [42], based on accurate numerical solutions of the Poisson–Boltzmann equation. For the results reported, solvation calculations were carried out at the gas-phase geometry of the small models using the 6-31G**/LACVP basis, employing a dielectric constant of $\varepsilon = 5$ to mimic the protein environment of the fibril. Free H^+ and Cu^{II}, on the other hand, were considered to be released into and obtained from an aqueous environment, respectively. Therefore, aqueous solvation energies reported in the literature were used in those cases [43, 44].

DFT calculations were also used to derive the QM gas-phase binding energies, which were then added to the solvation energies as described below. The overall free energy of copper binding for each peptide was calculated as

$$\Delta G_{\mathrm{B}} = E_{\mathrm{prep}} + \Delta E_{\mathrm{SCF}} - T\Delta S + \Delta G_{\mathrm{solv}},$$

where ΔG_{B} is total free energy of copper binding, E_{prep} is the MM peptide preparation energy (see "MD simulations"), ΔE_{SCF} is QM electronic binding energy, $\Delta S = S_{\mathrm{vib,complex}} - \Delta S_{\mathrm{trans}(Cu^{II})} - 3 \times S_{\mathrm{vib,His}} - S_{\mathrm{vib,oxygen\text{-}donor}}$, $\Delta S_{\mathrm{trans}(Cu^{II})}$ is the translational entropy of copper, calculated by the Sackur–Tetrode equation, and ΔG_{solv} is the QM solvation free energy of the small-model complex.

In addition to binding free energy components, the QM calculations also provided normal-mode force constants, which were used to design custom classical force fields for each complex, the details of which are given in the electronic supplementary material.

MD simulations

It has been shown experimentally that enforcing a lactam bond between Asp23 and Lys28 can dramatically accelerate the rate of folding of Aβ from the random coil found in solution to the β-sheet found in the fibrils [45]. We utilized this idea in our simulations. Starting from the NMR solution structure of Aβ42 (Protein Data Bank ID 1IYT) [46], we added the lactam bond as a constraint in gas-phase MD simulations at 320 K for 10 ns. It was found that after initial unfolding of the original NMR structure, which is α-helical in solution, the peptide refolded into a β-sheet after 4 ns and remained folded for the rest of the simulation time (see the electronic supplementary material). This folded β-sheet was the starting point for all our simulations. All seven possible complexes with different oxygen-donor ligands to copper were simulated for both Aβ42 and Aβ40 using the specially built force fields. Note that the metal–ligand force field derivation is highly nontrivial and tedious. These force fields are provided in the electronic supplementary material. The structures for Aβ40 were generated by removing the last two amino acids from the free Aβ42, equilibrating the structure for 1 ms, and generating all the copper-bound Aβ40s from this structure. The structural characteristics of the copper–Aβ complexes are discussed below. From these simulations, we obtained the protein preparation energy, E_{prep}, defined as the potential energy difference between the free peptide conformation and the folded peptide conformation constrained to bind copper. Since the two conformations used different force fields for MD simulations, their energies are not directly comparable. To enable comparison, the copper atom was removed and minimization using the same force field as for the free peptide was performed while imposing position restraints on the four atoms that coordinate copper. The position restrains were enforced by increasing the force constants for translation in each direction from 1,000 to 500,000 kJ mol^{-1} nm^{-1}.

All MD simulations used the MD package GROMACS version 3.2.1 [47]. Each MD simulation was preceded by a structural minimization run using the steepest-descent algorithm with an energy minimization tolerance of 1 kJ mol^{-1} nm^{-1}, with Lennard-Jones and Coulomb cut-offs set to 1.4 nm. The Leapfrog algorithm was used with a time integration step of 1 fs with no constraints, for a run duration of 1.5 ms using the structural constraint of a lactam bond, followed by another set of simulations for 1 ms without the lactam bond. All simulations were run in an NVT ensemble at a constant temperature of 320 K using the Berendsen algorithm for temperature coupling. Starting velocities were generated with a Maxwell–Boltzmann distribution corresponding to 320 K. All structures reported in this work were found to be stable within these MD runs. The simulation trajectories obtained were subjected to cluster analyses with the Jarvis–Patrick algorithm, and evaluation of the average minimized energy of the representative structure from each cluster at 100-ns time intervals further quantitatively confirmed the stability of each copper–peptide complex (see the electronic supplementary material).

Results and discussion

Small-model QM calculations

The DFT results show that the copper coordination geometry is distorted tetrahedral (Fig. 1b), which is common for four-coordinate d^9 metals. The calculated binding energies of the seven complexes, including the deprotonated forms of serine and tyrosine, are summarized in Table 1 (details are provided in the electronic supplementary material). Not surprisingly, the gas-phase enthalpies of binding (ΔH) show a dominant preference of the dicationic Cu^{II} center for anionic ligands. These energies are in the range 25–27 eV, whereas the neutral ligands give binding enthalpies of approximately 19 eV. The free ionic ligands are, of course, much better solvated and, thus, the solvation penalties for copper binding are substantially

Table 1 Quantum mechanical (QM) energies of small-model complexes

Complex	ΔH (eV)	ΔS (cal mol^{-1} K^{-1})	ΔG_{gas} (eV)	ΔG_{solv} (kcal mol^{-1})	ΔG_{BE} (QM) (kcal mol^{-1})
Cu^{II}–3His–Asp	−26.216	41.46	−26.752	521.85	*−95.06*
Cu^{II}–3His–Glu	−26.155	38.36	−26.651	520.70	*−93.86*
Cu^{II}–3His–Gln	−19.501	40.27	−20.021	400.25	*−61.44*
Cu^{II}–3His–Ser	−18.518	37.22	−18.999	392.78	−45.34
Cu^{II}–3His–Ser(−) + H$^+$	–	–	–	–	−49.01[a]
Cu^{II}–3His–Tyr	−18.711	44.75	−19.289	389.00	−46.81
Cu^{II}–3His–Tyr(−) + H$^+$	–	–	–	–	−61.84[a]

The most important lowest binding energies are highlighted in italic face

[a] Added free energy of deprotonation, calculated as $G_{\text{deprot}} = G_{\text{deprotonated complex}} + G_{\text{proton}} - G_{\text{protonated complex}}$

higher for these ligands than for neutral ligands. Our continuum solvation model assigns solvation penalties of approximately 520 and 390 kcal mol^{-1} for the anionic and neutral ligands, respectively, calculated in a low dielectric environment to mimic the protein environment of the fibril (Table 1). Combining all energy components, our small QM model identifies aspartate, glutamate, and glutamine as the most favorable ligands, with ΔG_{BE}(QM) estimates of −95.1, −93.9, and −61.4 kcal mol^{-1}, respectively. These highly negative binding energies are not physically meaningful, however, since they correspond to the free-energy change in bringing together four free ligands to form a complex with copper. In reality, the ligands are incorporated within the peptide framework, which must undergo a distortion to accommodate copper binding. This is expected to be an energetically uphill process that will counter the intrinsically favorable metal–ligand binding energy. The evaluation of this energy requires modeling the full-length peptide complexed with copper, which was carried out using classical MD.

MD simulations of Cu^{II}–Aβ complexes

There is agreement that residues 17–35 form a β-sheet in the solid phase and serve as hydrophobic contact points for building the fibril [48–50]. Experimentally, the formation of a lactam bond between Asp23 and Lys28 increased the rate of folding dramatically [45]. Using the same lactam bond in our simulations, we obtained a stable β-sheet after approximately 400 ps at 320 K. Using this structure as the initial guess, we simulated the seven possible copper-bound isomers for a total time of 2.5 ms after removing the auxiliary lactam bond. For the complexes containing serine and tyrosine as donor ligands, it was assumed that the structural distortions in their neutral and deprotonated forms would be similar and, therefore, only the neutral forms were simulated. Thus, the preparation energies of the neutral forms were used when calculating the overall binding energy of the complexes with the deprotonated forms, as shown in Table 3.

Initially, we anticipated that certain oxygen donors may give unreasonable structural deformations, but we found that plausible, stable structures could be obtained in our simulations for all oxygen donors in Aβ42; thus, we were unable to disqualify any of the isomers on structural grounds alone. On the other hand, in the case of Aβ40, the binding of several oxygen donors to copper resulted in unfolded structures, allowing us to discard those as unlikely candidates. It is important to emphasize that our simulations and predicted structure for the Aβs correspond to copper binding in solid phase in which the peptides are organized in fibrils, since the β-sheet structure is the dominant form only in the fibril. In the solution phase, Aβ42/Aβ40 is likely to adopt a much less defined structure [15]. Our simulated structures of the copper-bound Aβ allow estimation of the energy required to distort the peptide to give the structure that it adopts when copper is bound. This preparation energy, E_{prep}(MM), calculated using classical mechanics, was computed as the difference in potential energy between the distorted peptide after deleting the copper and the free peptide. Both were evaluated using the standard Gromos [47, 51] force field. The average potential energy of each complex in 100-ns increments for the final 1 ms is shown in Table 2 (see the electronic supplementary material for details). E_{prep} was calculated as the average potential energy of each complex relative to the average energy of the free peptides. Note that this analysis also demonstrates the convergence of the potential energy as the simulation progresses, as judged by the reduced fluctuations of the potential energies in each increment (less than 15 kcal mol^{-1} in most cases).

Adding the small-model QM and full-peptide MM energies gives the total free energy of binding copper, shown in Table 3. As highlighted in the table, Tyr10 is the best oxygen-donor ligand in Aβ42, with ΔG_{BE} of −8.8 and −23.8 kcal mol^{-1} for the neutral and the deprotonated

Table 2 Potential energies of each copper–Aβ complex at 100-ns intervals in kcal mol^{-1}

Complex	Average potential energy	E_{prep} Cu–Aβ42	Average potential energy	E_{prep} Cu–Aβ40
Aβ free	−996.11	0.00	−1,017.79	0.00
Cu(II)–3His–Asp1	−905.56	90.55	−842.13	175.67
Cu(II)–3His–Asp7	−895.40	100.70	−866.81	150.98
Cu(II)–3His–Glu3	−881.38	114.72	−728.35	289.44
Cu(II)–3His–Glu11	−891.66	104.44	−867.50	150.29
Cu(II)–3His–Ser8	−906.32	89.79	−922.40	95.40
Cu(II)–3H–Tyr10	−958.10	38.01	−889.84	127.95
Cu(II)–3His–Gln15	−933.48	62.63	−952.08	65.71

The *second* and *third* columns enumerate results for the Aβ42 and the *fourth* and *fifth* columns list results for the Aβ40 complexes

Table 3 Summary of energy components from QM and molecular mechanical calculations in kilocalories per mole

Complex	ΔG_{sol}(QM)	E_{prep} Aβ42	ΔG_{BE} Aβ42	E_{prep} Aβ40	ΔG_{BE} Aβ40
Cu^{II}–3His–Asp1	−95.06	90.55	*−4.51*	175.67	80.61
Cu^{II}–3His–Asp7	−95.06	100.70	5.64	150.98	55.92
Cu^{II}–3His–Glu3	−93.86	114.72	20.86	289.44	195.58
Cu^{II}–3His–Glu11	−93.86	104.44	10.58	150.29	56.43
Cu^{II}–3His–Ser8	−45.34	89.79	44.45	95.40	50.06
Cu^{II}–3His–Ser8(−) + H^+	−49.01	89.79	40.78	95.40	46.39
Cu^{II}–3His–Tyr10	−46.81	38.01	*−8.80*	127.95	81.14
Cu^{II}–3His–Tyr10(−) + H^+	−61.84	38.01	*−23.83*	127.95	66.11
Cu^{II}–3His–Gln15	−61.44	62.63	1.19	65.71	*4.27*

The lowest binding energies are in *italics*

forms, respectively, followed by Asp1, which has ΔG_{BE} of −4.5 kcal mol^{-1}. Because of the approximate way the deprotonation process is treated, the absolute binding energy of the deprotonated Tyr10(−) ligand is likely exaggerated, but the trend should be physically meaningful. A close examination of the energy components reveals the substantial contribution of E_{prep}, which overrides the intrinsically strong metal–ligand bonding of the anionic oxygen-donor ligands Glu3, Asp7, and Asp11 to favor Tyr10 binding, which has the lowest E_{prep} value, stressing that considering only metal–ligand bonding is not good enough. The fact that the binding energy of Asp1 is also negative suggests that it may also be a viable oxygen-donor ligand and that Tyr10 and Asp1 may even coexist in equilibrium. Another logical consequence is that depending on the experimental conditions, Tyr10 or Asp1 may be the dominant copper binding ligand, providing a plausible rationale for why it is exceedingly difficult to unambiguously characterize the ligand environment of the copper–Aβ complex. Tyr10 was previously proposed to be the oxygen-donor ligand on the basis of Raman spectroscopy [30], but our study is the first to offer comparative computational support for this notion. Moreover, in vitro studies showed that rat Aβ, which contains the mutations R5G, Y10F, and H13R, displays greatly decreased metal binding to Cu^{II} and Zn^{II}, and generation of hydrogen peroxide [7, 52].

The results for Aβ40 show striking differences compared with those for Aβ42. While all binding energies are found to be positive in this case, suggesting that none of the ligands form stable complexes with copper, Gln15 has the lowest relative binding energy and is expected to be the most likely ligand. It is also one of the three complexes that remains folded in the β-sheet conformation (see the electronic supplementary material). Moreover, Gln15 and Ser8 are the only oxygen-containing residues among the first 16 residues of Aβ that were not included in the mutagenesis studies of Karr et al. [11] and, therefore, were not eliminated as potential ligands. In contrast to our results, experimental evidence shows that Aβ40 does bind copper, although with a lower affinity compared with Aβ42. Thus, our results are quantitatively in disagreement with experimental evidence and a qualitative interpretation of our data may be more appropriate. Alternatively, our approach of modeling Aβ40 by truncating the last two amino acids from the prefolded structure of Aβ42 may not be valid, since it is possible that Aβ40 adopts a different β-sheet conformation. In any case, our results suggest that Aβ42 and Aβ40 display very different chemical behavior toward copper binding.

Figure 3 compares the structures of free Aβ42 and Aβ40, as well as their copper-bound forms with the lowest-energy structures using Tyr10 and Gln15 as ligands, respectively. As can be seen from the illustrations, the C-terminal ends of the peptides interact with the hydrophilic N-terminal end, which houses the copper-binding residues. These interactions between the C-terminal end and the N-teminal residues play an active role in stabilizing the peptides and in the thermodynamics of reorganization for copper binding. Specifically, for free Aβ42, the β-turn causes the C-terminal end to be close to Tyr10, while in the case of the copper-bound structure we observe a "slippage" of the β-sheet to expose His13 and His14 for copper binding, such that the C-terminal end now interacts with Lys16. In the case of Aβ40 on the other hand, there is not much "slippage," with the C-terminal end interacting with Lys16 in both cases. Note that our predicted structure of free Aβ40 is in close overall agreement with constraints from solid-state NMR, in particular the close proximity of the C-terminal end with His14 [49]. Consequently, the lowest-energy conformations for Aβ40 and Aβ42 are not identical for a fundamental reason. These results suggest that the widely adopted notion that the smaller peptides Aβ16, Aβ28, and Aβ40 are good models for Aβ42, since the ligands that are directly involved in copper binding are all present, may have to be reevaluated.

Figure 4 shows a representative structure of the copper–Aβ42 complex with Tyr10 as a ligand. The coordination

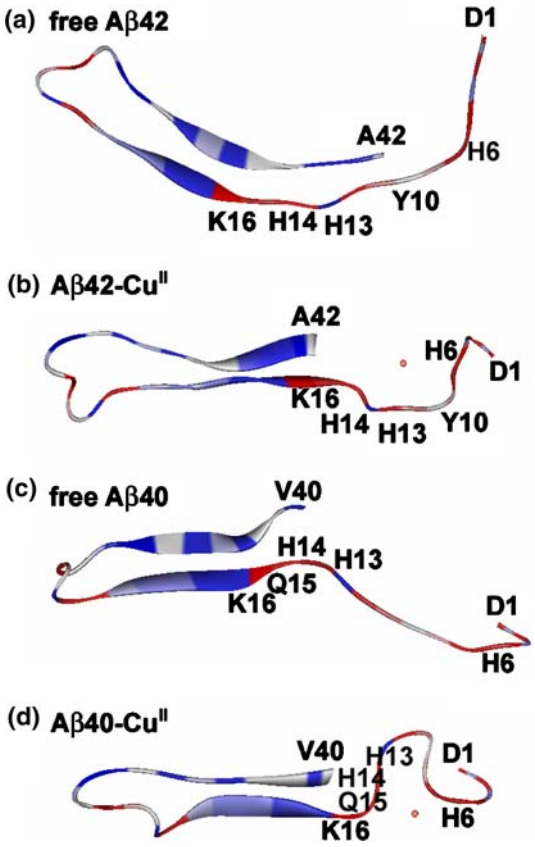

Fig. 3 Ribbon representations of structures of free and copper-bound peptides: **a** free Aβ42, **b** Aβ42 with His6, His13, His14, and Tyr10 bound to copper, **c** free Aβ40, **d** Aβ40 with His6, His13, His14, and Gln15 bound to copper. The *ribbons* are colored according to hydrophobicity. The amino acids bound to copper, those that mark the N- and C-termini, and Lys16 (which marks the end of the N-terminal hydrophilic region) are labeled

geometry around copper is distorted tetrahedral, and the copper atom sits in a pocket formed by the flexible N-terminal region of the peptide. Residues from Leu17 onward are stabilized through intramolecular hydrogen bonding, with residues 19–21 and 36–38 forming the core of the β-sheet. There is a strong hydrogen bond between Tyr10 and Glu3 (H···O 1.54 Å), which may assist in deprotonating the phenolic hydroxyl group and increase its basicity toward copper. This binding mode may also provide an alternative explanation for the results observed by Karr et al. [11]. In their study, the EPR spectra of native copper-bound Aβ40 and a mutant with the first three N-terminal residues deleted were compared and found to be different. On the basis of this observation, it was concluded that the N-terminal residues were important in forming the native copper-binding environment, possibly comprising one of the ligands. On the basis of our simulations, however, those results can also be interpreted as the loss of a hydrogen-bonding interaction to a copper ligand, which may affect the coordination geometry and binding affinity.

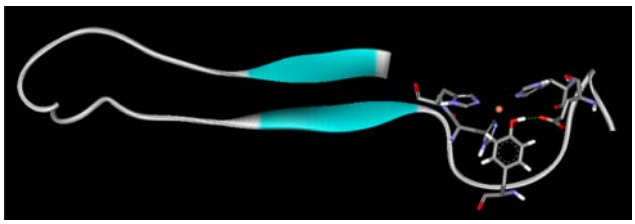

Fig. 4 Ribbon representation of the lowest-energy conformation of copper bound to Aβ42. The four ligands to copper, His6, His13, His14, and Tyr10, and Glu3, which forms a hydrogen bond with Tyr10, are shown in stick form, while all other atoms are hidden for clarity

A more recent report by Karr and Szalai [32] has suggested a similar model based on the pH dependence of their copper–Aβ16 EPR spectra, although their model suggests the involvement of Asp1 in such hydrogen bonding.

In conclusion, we have used a combination of DFT and classical MD simulations to compare the binding energies of nine possible oxygen-donor ligands and identified Tyr10 and Asp1 to be the most likely fourth ligands of Cu^{II} in Aβ42. The same protocol applied to Aβ40 suggests Gln15 as the most likely candidate. More importantly, Tyr10, which is the most favored ligand in Aβ42, causes unfolding of the β-sheet structure in Aβ40. This inconsistency suggests the need for a reevaluation of the assumption that the shorter peptides can be used as accurate models of Aβ42. Aβ40 is often preferred in experimental studies because it is less prone to aggregation and, therefore, easier to handle. Our results suggest that the additional two C-terminal residues make Aβ42 very different from Aβ40, especially in their copper-bound forms. This perspective may also resolve several discrepancies between groups of researchers that have attempted to identify the fourth ligand. While there is evidence both for [8, 19, 30, 31] and against [11, 13, 15, 17, 32, 53–55] Tyr10 being the fourth ligand, most of those studies were done using either Aβ42 monomers in the solution phase or Aβ40 and shorter peptides. An exception is the work of Dong et al. [55], which was carried out on senile plaques using Aβ42 and which also found no evidence for Tyr10 coordination to copper; however, that study did not report on the copper coordination environment, except that histidine was involved in coordination. Thus, there is little evidence for the binding mode of Aβ42 in those plaques being the native 3N1O type. On the basis of our current results, we propose that the binding mode of Aβ42 is different from that of the smaller peptides, and thus studies that were carried out using smaller peptides such as Aβ16, Aβ28, and Aβ40 may provide limited insight for understanding the chemistry of Aβ42.

Whereas other structural motifs such as 4N binding or the involvement of the N-terminus and/or oxygen donors

from the peptidyl backbone have also been proposed in various models and must be tested in the future, the high-precision structures that we obtained now allow for a critical assessment of the catalytic dioxygen activation mechanism using high-resolution QM techniques. Lastly, this work highlights how small changes at presumably remote sites of the peptide can dramatically alter the chemistry that is displayed.

Acknowledgments We thank NSF (0116050 and CHE-0645381) for financial support. We also thank the Research Corporation for a Cottrell Award (M.-H.B.), the Alfred P. Sloan Foundation for an Alfred P. Sloan Fellowship (M.-H.B) and Iris Klinkenberg for a Klinkenberg Award (Y.M.).

References

1. Varadarajan S, Yatin S, Aksenova M, Butterfield DA (2000) J Struct Biol 130:184–208
2. Pike CJ, Walencewicz AJ, Glabe CG, Cotman CW (1991) Brain Res 563:311–314
3. Hardy J, Selkoe DJ (2002) Science 297:353–356
4. Bush AI, Pettingell WH, Multhaup G, Paradis MD, Vonsattel JP, Gusella JF, Beyreuther K, Masters CL, Tanzi RE (1994) Science 265:1464–1467
5. White AR, Multhaup G, Maher F, Bellingham S, Camakaris J, Zheng H, Bush AI, Beyreuther K, Masters CL, Cappai R (1999) J Neurosci 19:9170–9179
6. Atwood CS, Scarpa RC, Huang XD, Moir RD, Jones WD, Fairlie DP, Tanzi RE, Bush AI (2000) J Neurochem 75:1219–1233
7. Huang XD, Cuajungco MP, Atwood CS, Hartshorn MA, Tyndall JDA, Hanson GR, Stokes KC, Leopold M, Multhaup G, Goldstein LE, Scarpa RC, Saunders AJ, Lim J, Moir RD, Glabe C, Bowden EF, Masters CL, Fairlie DP, Tanzi RE, Bush AI (1999) J Biol Chem 274:37111–37116
8. Barnham KJ, Haeffner F, Ciccotosto GD, Curtain CC, Tew D, Mavros C, Beyreuther K, Carrington D, Masters CL, Cherny RA, Cappai R, Bush AI (2004) FASEB J 18:1427–1429
9. Barnham KJ, McKinstry WJ, Multhaup G, Galatis D, Morton CJ, Curtain CC, Williamson NA, White AR, Hinds MG, Norton RS, Beyreuther K, Masters CL, Parker MW, Cappai R (2003) J Biol Chem 278:17401–17407
10. Rossjohn J, Cappai R, Feil SC, Henry A, McKinstry WJ, Galatis D, Hesse L, Multhaup G, Beyreuther K, Masters CL, Parker MW (1999) Nat Struct Biol 6:327–331
11. Karr JW, Akintoye H, Kaupp LJ, Szalai VA (2005) Biochemistry 44:5478–5487
12. Karr JW, Kaupp LJ, Szalai VA (2004) J Am Chem Soc 126:13534–13538
13. Syme CD, Nadal RC, Rigby SEJ, Viles JH (2004) J Biol Chem 279:18169–18177
14. Curtain CC, Ali F, Volitakis I, Cherny RA, Norton RS, Beyreuther K, Barrow CJ, Masters CL, Bush AI, Barnham KJ (2001) J Biol Chem 276:20466–20473
15. Raffa DF, Rauk A (2007) J Phys Chem B 111:3789–3799
16. Gomez-Balderas R, Raffa DF, Rickard GA, Brunelle P, Rauk A (2005) J Phys Chem A 109:5498–5508
17. Rickard GA, Gomez-Balderas R, Brunelle P, Raffa DF, Rauk A (2005) J Phys Chem A 109:8361–8370
18. Barnham KJ, Haeffner F, Ciccotosto GD, Curtain CC, Tew D, Masters CL, Chemy RA, Cappai R, Bush AI (2004) Neurobiol Aging 25:S544
19. Haeffner F, Smith DG, Barnham KJ, Bush AI (2005) J Inorg Biochem 99:2403–2422
20. Baumketner A, Bernstein SL, Wyttenbach T, Bitan G, Teplow DB, Bowers MT, Shea J-E (2006) Protein Sci 15:420–428
21. Baumketner A, Bernstein SL, Wyttenbach T, Lazo ND, Teplow DB, Bowers MT, Shea J-E (2006) Protein Sci 15:1239–1247
22. Jang S, Shin S (2008) J Phys Chem B 112:3479–3484
23. Itoh SG, Okamoto Y (2008) J Phys Chem B 112:2767–2770
24. Shen L, Ji H-F, Zhang H-Y (2008) J Phys Chem B 112:3164–3167
25. Triguero L, Singh R, Prabhakar R (2008) J Phys Chem B 112:2159–2167
26. Jiao Y, Yang P (2007) J Phys Chem B 111:7646–7655
27. Li W, Zhang J, Su Y, Wang J, Qin M, Wang W (2007) J Phys Chem B 111:13814–13821
28. Rauk A (2008) Dalton Trans 1273–1282
29. Dong X, Chen W, Mousseau N, Derreumaux P (2008) J Chem Phys 128:125108
30. Miura T, Suzuki K, Kohata N, Takeuchi H (2000) Biochemistry 39:7024–7031
31. Atwood CS, Perry G, Zeng H, Kato Y, Jones WD, Ling KQ, Huang XD, Moir RD, Wang DD, Sayre LM, Smith MA, Chen SG, Bush AI (2004) Biochemistry 43:560–568
32. Karr JW, Szalai VA (2007) J Am Chem Soc 129:3796–3797
33. Kim W, Hecht MH (2005) J Biol Chem. M505763200
34. Bitan G, Kirkitadze MD, Lomakin A, Vollers SS, Benedek GB, Teplow DB (2003) Proc Natl Acad Sci USA 100:330–335
35. Parr RG, Yang W (1989) Density functional theory of atoms and molecules. Oxford University Press, New York
36. Schrödinger (2003) Jaguar 5.5. Schrödinger, Portland
37. Becke AD (1988) Phys Rev A 38:3098–3100
38. Becke AD (1993) J Chem Phys 98:5648–5652
39. Lee CT, Yang WT, Parr RG (1988) Phys Rev B 37:785–789
40. Hay PJ, Wadt WR (1985) J Chem Phys 82:299–310
41. Dunning TH (1989) J Chem Phys 90:1007–1023
42. Marten B, Kim K, Cortis C, Friesner RA, Murphy RB, Ringnalda MN, Sitkoff D, Honig B (1996) J Phys Chem 100:11775–11788
43. Marcus Y (1991) J Chem Soc Faraday Trans 87:2995–2999
44. Tawa GJ, Topol IA, Burt SK, Caldwell RA, Rashin AA (1998) J Chem Phys 109:4852–4863
45. Sciarretta KL, Gordon DJ, Petkova AT, Tycko R, Meredith SC (2005) Biochemistry 44:6003–6014
46. Crescenzi O, Tomaselli S, Guerrini R, Salvadori S, D'Ursi AM, Temussi PA, Picone D (2002) Eur J Biochem 269:5642–5648
47. Van Der Spoel D, Lindahl E, Hess B, Groenhof G, Mark AE, Berendsen HJ (2005) J Comput Chem 26:1701–1718
48. Antzutkin ON, Leapman RD, Balbach JJ, Tycko R (2002) Biochemistry 41:15436–15450
49. Petkova AT, Ishii Y, Balbach JJ, Antzutkin ON, Leapman RD, Delaglio F, Tycko R (2002) Proc Natl Acad Sci USA 99:16742–16747
50. Esler WP, Stimson ER, Ghilardi JR, Lu Y-A, Felix AM, Vinters HV, Mantyh PW, Lee JP, Maggio JE (1996) Biochemistry 35:13914–13921
51. Berendsen HJC, Vanderspoel D, Vandrunen R (1995) Comput Phys Commun 91:43–56
52. Huang XD, Atwood CS, Hartshorn MA, Multhaup G, Goldstein LE, Scarpa RC, Cuajungco MP, Gray DN, Lim J, Moir RD, Tanzi RE, Bush AI (1999) Biochemistry 38:7609–7616
53. Kowalik-Jankowska T, Ruta M, Wisniewska K, Lankiewicz L (2003) J Inorg Biochem 95:270–282
54. Schoneich C, Williams TD (2002) Chem Res Toxicol 15:717–722
55. Dong J, Atwood CS, Anderson VE, Siedlak SL, Smith MA, Perry G, Carey PR (2003) Biochemistry 42:2768–2773